DOE/ER/40561-334-INT96-21-07
CU-TH-857

Transverse Energy Evolution as a Test of Parton Cascade Models [0]

Miklos Gyulassy[1,2], Yang Pang[1,3], and Bin Zhang[1,2]

1.Department of Physics, Columbia University, New York, NY 10027 USA
2.INT, University of Washington, Box 351550 Seattle, WA 98195, USA
3. Brookhaven National Laboratory, Upton, New York, 11973

Abstract

We propose a test of Monte Carlo Parton Cascade models based on analytic solutions of covariant kinetic theory for longitudinally boost and transverse translation invariant boundary conditions. We compute the evolution of the transverse energy per unit rapidity for typical mini-jet initial conditions expected in ultra-relativistic nuclear collisions. The kinetic theory solutions under these conditions test the models severely because they deviate strongly from free-streaming and also from ideal Euler and dissipative Navier-Stokes hydrodynamical approximations. We show that the newly formulated ZPC model passes this test. In addition, we show that the initial mini-jet density would need to be approximately four times higher than estimated with the HIJING generator in central Au+Au collisions at c.m. energies 200 AGeV in order that parton cascade dynamics can be approximated by Navier-Stokes hydrodynamics.

[0] PREPARED FOR THE U.S. DEPT. OF ENERGY UNDER GRANTS DE-FG06-90ER40561, DE-FG02-93ER40764, DE-FG-02-92-ER40699, and DE-AC02-76CH00016.

1 Introduction

Monte Carlo parton cascade models [1, 2, 3, 4, 5, 6, 7, 8, 9] are currently being developed to calculate multiparticle production and evolution in ultra-relativistic nuclear collisions. These are being written in a new Open Standard Codes and Routines (OSCAR) format[10] to enable rigorous testing of essential components of the algorithms and insure reproducibility of the numerical results. Given the present large uncertainties in the formulation of QCD kinetic theory and in the validity of algorithms employed to simulate off-shell propagation, screening effects, color coherence, parton production and absorption, and hadronization, it is important to develop and subject codes to standardized tests on problems where analytic solutions are known. One reason for concern is that cascade models necessarily violate Lorentz invariance through the scattering prescriptions involving action at a distance [11, 12, 13, 14, 15]. At RHIC and LHC energies, the phase space of partons span over ten units of rapidity and extreme Lorentz contraction effects arise which amplify non-causal numerical artifacts. Numerical prescriptions have been proposed to minimize such Lorentz violations effects[15]. However, without further tests it is impossible to ascertain whether the final numerical results are in fact physically correct. Different Monte-Carlo event generators can give different predictions even for basic observables such as the transverse energy per unit rapidity, $dE_\perp/dy$.

In this paper we propose a simple test of the multiple collision algorithm of such models through the computation of the evolution of $dE_\perp/dy$ in the special case of longitudinal boost and transverse translation invariant thermal initial conditions. This observable is of interest because it is the simplest one sensitive to collective hydrodynamic phenomena. It is known[16] that for such boundary conditions, Euler hydrodynamics predicts that the final observed transverse energy is reduced by a factor of about two relative to the initial value due to pdV work associated with longitudinal expansion[17]. This very basic feature of ultra-relativistic nuclear reactions arises even if the initial conditions are highly inhomogeneous and turbulent as shown recently in [18]. On the other hand, pQCD estimates suggest that the viscosity of a quark gluon plasma is very high, and Navier-Stokes hydrodynamic equations predict about a factor of two less work is done by the plasma. The observable consequence of such dissipative dynamics is the reduction of the transverse energy loss predicted by Euler hydrodynamics[19, 20]. In fact,the parton

mean free paths may be so long that even the Navier-Stokes approximation. It appears essential therefore to employ a full microscopic transport theory to evaluate precisely the magnitude of that transverse energy loss. The newly developed parton cascade models provide an approximate numerical solution to the underlying covariant transport theory and are thus ideally suited to address this problem.

In [21, 22, 23] analytic solutions for the evolution of the energy density were found using relativistic Boltzmann kinetic theory[24]. In this paper we extend those solutions to initial conditions more relevant to the RHIC energy domain and propose these to test parton cascade models.

The discussion is organized as follows: In section 2, we review essential elements of longitudinally boost invariant kinetic theory. The free streaming solution is discussed for both the ideal inside-outside and local thermal initial conditions. The integral equation for the phase space distribution in the relaxation time approximation is presented. In section 3, the integral equation for the energy density is derived together with its Navier-Stokes limit for both constant and scaling relaxation times. In section 4, the integral equation for the transverse energy evolution is derived and solved numerically. The results show that for the expected initial conditions based on the HIJING event generator[3], kinetic theory leads to much less collective transverse energy loss than Euler hydrodynamics but more than Navier-Stokes. We show that at least one of the newly developed models, ZPC[15], is able to pass this test. Finally, we show that the ZPC also reproduces the kinetic theory solution under more extreme conditions where the kinetic theory solution approaches the Navier-Stokes solution. As far as we know, this is the first demonstration of a parton cascade solution approaching an analytic Navier-Stokes result. Physically, this result is of interest because it shows that in order to approach the Navier-Stokes regime initial parton densities must be at least a factor of four greater than predicted by the HIJING event generator[3] for central $Au + Au$ collisions at RHIC.

2 Boost Invariant Relativistic Transport

The covariant kinetic equation for the invariant on-shell phase space density, $f(x,p)$ is

$$(p\partial_x)f(x,p) = (pu)(C(x,p) + S(x,p)) \tag{1}$$

where C is the Boltzmann collision term, S is the source term, and u^μ is the collective flow velocity field. This equation greatly simplifies in the case that longitudinal boost invariance and transverse translation invariance is assumed[21, 22, 23]. In that case, the on-shell phase space distribution function depends only on the reduced phase space variables $(\tau, \xi, \mathbf{p}_\perp)$, where $\tau^2 = t^2 - z^2$ and $\xi = \eta - y$ in terms of the kinetic rapidity $y = \tanh^{-1}(p^z/p^0)$ and pseudo-rapidity $\eta = \tanh^{-1}(z/t)$. The collective flow velocity field in this case is $u^\mu = x^\mu/\tau = (\mathrm{ch}\eta, 0_\perp, \mathrm{sh}\eta)$ with $(pu) = m_\perp \mathrm{ch}\xi$ and the transport equation reduces to

$$\begin{aligned}(p\partial_x) f(x,p) &= m_\perp \left(\mathrm{ch}(\xi) \frac{\partial}{\partial \tau} - \frac{\mathrm{sh}(\xi)}{\tau} \frac{\partial}{\partial \xi} \right) f(\tau, \xi, \mathbf{p}_\perp) \\ &= (pu) \frac{d}{d\tau} f(\tau, \bar{\xi}(\tau), \mathbf{p}_\perp) \ . \end{aligned} \tag{2}$$

The characteristic function $\bar{\xi}(\tau) \equiv \bar{\xi}(\tau; \tau_0, \xi)$ satisfies

$$d\bar{\xi}/d\tau = -\tau^{-1} \tanh \bar{\xi} \ , \tag{3}$$

and passes through $\xi = \bar{\xi}(\tau_0; \tau_0, \xi)$ at $\tau = \tau_0$. This trajectory satisfies

$$\begin{aligned} t\, \mathrm{sh}\bar{\xi}(t; \tau, \xi) &= \tau\, \mathrm{sh}\xi \\ \mathrm{ch}\bar{\xi}(t; \tau, \xi) &= \left(1 + (\tau/t)^2 \mathrm{sh}^2 \xi\right)^{1/2} \ . \end{aligned} \tag{4}$$

We will drop the τ or ξ arguments on $\bar{\xi}(t)$ when confusion cannot arise.

In [22] the source of partons was modeled by a Schwinger pair production. That mechanism models soft beam jet fragmentation for lab energies < 200 AGeV. At ultra-relativistic collider energies $\sqrt{s} > 100$ AGeV, perturbative QCD minijet production is currently thought to dominate the parton production mechanism [3, 20]. Given an initial distribution of massless partons, e.g. from HIJING[3],

$$g(y, \mathbf{p}_\perp) = dN_g/dy d^2p_\perp \ , \tag{5}$$

the first problem is to construct the source phase space distribution, $S(x, p)$.

2.1 Free Streaming Case

To construct the source, consider an ensemble of on-shell partons with production phase space coordinates, $\{x_a^\mu, p_a^\mu; p_a^2 = m^2\}$. The general form of the covariant free streaming phase space distribution is given by [24]

$$\mathcal{F}(x,p) \;=\; \int ds \langle \sum_a P(s,p_a)\delta^4(x^\mu - x_a^\mu - p_a^\mu s)\delta^4(p-p_a)\rangle \;\;, \tag{6}$$

where $P(s,p)$ is introduced as the Lorentz scalar probability that a parton with four momentum p has been formed by proper time $\tau = s\ m$. This of course depends on details of the formation dynamics and external four vectors and parameters specifying the reaction.

The on-shell constraint leads to

$$\delta^4(p-p_a) \;=\; 2\theta(p_0)\delta(p^2-m^2)\delta(y-y_a)\delta^2(\mathbf{p}_\perp - \mathbf{p}_{\perp a}) \;\;, \tag{7}$$

and thus the reduced (6+1) dimensional phase space density, f, is defined through

$$\mathcal{F}(x,p) = 2\theta(p^0)\delta(p^2-m^2)f(x,p) \;\;. \tag{8}$$

The on-shell phase space source function in eq.(1) is then given by

$$S(x,p) = \frac{1}{(pu)}(p\partial_x)f(x,p) \;\;. \tag{9}$$

For boost invariant boundary conditions,

$$S(\tau,\xi,\mathbf{p}_\perp) = \frac{d}{d\tau} f(\tau, \bar{\xi}(\tau,\tau',\xi)), \mathbf{p}_\perp)|_{\tau'=\tau} \;\;. \tag{10}$$

The local energy-momentum tensor and parton current are obtained as [24]

$$\begin{aligned} T^{\mu\nu}(x) \;&=\; \int d^4p\ p^\mu p^\nu \mathcal{F}(x,p) = \int \frac{d^3\mathbf{p}}{p^0}\ p^\mu p^\nu f(x,p) \\ J^\mu(x) \;&=\; \int d^4p\ p^\mu \mathcal{F}(x,p) = \int \frac{d^3\mathbf{p}}{p^0}\ p^\mu f(x,p) \;\;. \end{aligned} \tag{11}$$

The proper energy density and number density are in turn given by $\epsilon(x) = u_\mu u_\nu T^{\mu\nu}(x)$, $\rho(x) = u_\mu J^\mu(x)$ We use here the Landau definition [24] of the

normalized fluid four velocity $u^\mu(x) = T^{\mu\nu}u_\nu/(uTu)$, such that the energy flux, T^{0i}, vanishes in the comoving frame where $u^\mu = (1,0,0,0)$.

The central observable of interest is the parton invariant momentum distribution as given by the Cooper-Frye formula

$$E\frac{d^3N}{d^3p} = \int_\Sigma d\Sigma_\mu p^\mu f(x,p) \tag{12}$$

Here $\Sigma^\mu(\zeta_1,\zeta_2,\zeta_3)$ specifies the 3D hypersurface on which the momentum distribution is measured. The volume element is given by

$$d\Sigma_\mu = \epsilon_{\mu\alpha\beta\gamma}(\partial\Sigma^\alpha/\partial\zeta_1)(\partial\Sigma^\beta/\partial\zeta_2)(\partial\Sigma^\gamma/\partial\zeta_3)d\zeta_1 d\zeta_2 d\zeta_3 \ .$$

For a fixed time measurement, we take $(\zeta_1,\zeta_2,\zeta_3) = (\mathbf{x}_\perp, z)$, $\Sigma^\mu = x^\mu = (t, z, \mathbf{x}_\perp)$ so that $d\Sigma_\mu = (d^3x, \mathbf{0})$. The inclusive parton distribution at time t is then given by

$$E\frac{d^3N}{d^3p}(t) \ = \ \frac{dN(t)}{dyd^2\mathbf{p}_\perp} = E\int d^3x f(x,p) \ , \tag{13}$$

and the transverse energy per unit rapidity at time t is

$$\frac{dE_\perp(t)}{dy} \ = \ \int d^2\mathbf{p}_\perp \ m_\perp \frac{dN}{dyd^2\mathbf{p}_\perp} \ . \tag{14}$$

On the other hand, for the physically more relevant longitudinal boost invariant boundary conditions, the final parton distribution requires an integration over a fixed proper time freeze-out surface. For $\tau = (t^2 - z^2)^{1/2} = \tau_f$, Σ is conveniently parameterized by $\Sigma^\mu = (\tau_f \mathrm{ch}\eta, \tau_f \mathrm{sh}\eta, \mathbf{x}_\perp)$ with $d\Sigma^\mu = (\tau_f \mathrm{ch}\eta, -\tau_f \mathrm{sh}\eta, 0)d\eta d\mathbf{x}_\perp$. Therefore, $d\Sigma^\mu p_\mu = (\tau_f m_\perp \mathrm{ch}\xi)d\eta d\mathbf{x}_\perp$. In this case,

$$\frac{dN(\tau_f)}{dyd^2\mathbf{p}_\perp} = \int \tau_f d\eta d^2\mathbf{x}_\perp \ m_\perp \mathrm{ch}\xi \ f(x,p) \ , \tag{15}$$

and the basic calorimetric observable is

$$\mathrm{e}_\perp(\tau_f) \ \equiv \ \frac{dE_\perp(\tau_f)}{dy} = \int \tau_f d\eta d^2\mathbf{x}_\perp \int d^2\mathbf{p}_\perp m_\perp^2 \mathrm{ch}\xi \ f(x,p) \tag{16}$$

Our main focus here is on how $\mathrm{e}_\perp(\tau)$ evolves to its final form given an initial boost invariant value at $\tau = \tau_0$.

2.2 Ideal Inside-Outside Correlation

In nuclear collisions at ultra-relativistic energies, the initial parton coordinates are approximately localized on a transverse sheet, with $x_a^\mu = (0, \mathbf{x}_{\perp a}, 0)$ with $\mathbf{x}_{\perp a}$ distributed over a transverse area according to a density $\rho(\mathbf{x}_\perp) \approx \theta(R-r)/\pi R^2$. Transforming to the $(\tau, \xi = \eta - y, \mathbf{p}_\perp)$ coordinates

$$\delta^4(x - x_a - ps) \;=\; \frac{\delta(\xi)}{m_\perp \tau}\delta(s - \tau/m_\perp)\delta^2(\mathbf{x}_\perp - \mathbf{x}_{\perp a} - \frac{\mathbf{p}_\perp}{m_\perp}\tau) \;\; . \qquad (17)$$

Neglecting transverse expansion, the approximate ideal inside-outside correlated distribution is given by

$$f_0(\tau, \xi, p_\perp) \;\approx\; \frac{\delta(\xi)}{m_\perp \tau \pi R^2} P(\tau m_\perp) g(\mathbf{p}_\perp) \qquad (18)$$

The influence of the formation physics can be studied by comparing two analytic models of $P = P(m_\perp \tau)$:

$$P(m_\perp \tau) = \begin{cases} \theta(\tau - \tau_0) & Model\ I \\ (m_\perp \tau)^2/(1 + (m_\perp \tau)^2) & Model\ II \end{cases} \qquad (19)$$

Model I is simplest for analytic tests, while Model II is more realistic based on a study [25] of induced radiation in multiple collisions. This is obviously one of the most uncertain aspects of parton cascade models since formation physics is beyond the scope of ballistic kinetic theory. At the least, kinetic theory could be supplemented by classical field evolution such as proposed in[26]. (See [20] for example for solutions to coupled field and kinetic equations in the chromo-hydrodynamics limit.)

The phase space source function given (18) is

$$S_0(x,p) = \frac{d}{d\tau}\frac{\delta(\bar{\xi}(\tau))P(m_\perp\tau)}{m_\perp \tau \pi R^2} g(\mathbf{p}_\perp) = \frac{\delta(\xi)\dot{P}(m_\perp \tau)}{\tau \pi R^2} g(\mathbf{p}_\perp) \;\; , \qquad (20)$$

where we used

$$\delta(\bar{\xi}(t;\tau,\xi)) = \frac{t}{\tau}\delta(\xi) \;\; . \qquad (21)$$

For this ideal $\xi = 0$ correlated case, the energy-momentum tensor has the form $T_0^{\mu\nu}(x) u^\mu u^\nu \epsilon_0(\tau) + \delta_\perp^{\mu\nu} P_T(\tau)$ where $\delta_T^{\mu\nu} = \mathrm{diag}(0,0,1,1)$. The proper energy density evolves as

$$\epsilon_0(\tau) = (uTu) = \frac{\langle m_\perp P(m_\perp \tau)\rangle}{\tau \pi R^2} \;\; , \qquad (22)$$

where the brackets are used to indicate the transverse momentum integration $\langle \cdots \rangle \equiv \int d^2\mathbf{p}_\perp \; g(\mathbf{p}_\perp) \cdots$ Note that for the ideal correlated case, the proper longitudinal pressure vanishes, while the transverse pressure, $P_T = \epsilon/2$, is 50% larger than in thermal equilibrium for massless partons.

The hydrodynamic equations follow from $((\partial T)u) = \sigma$ where

$$\sigma(\tau) = \int d\xi d^2\mathbf{p}_\perp m_\perp^2 \mathrm{ch}\xi^2 S(\tau, \xi, \mathbf{p}_\perp) \tag{23}$$

is the proper energy density source per unit time. The proper energy density evolves as

$$\dot{\epsilon} + \frac{\epsilon}{\tau} = \sigma(\tau) = \frac{\langle m_\perp^2 \dot{P}(m_\perp \tau)\rangle}{\tau \pi R^2} \tag{24}$$

The well known solution is given by $\epsilon(\tau) = \epsilon_0(\tau)$ from eq.(22). For the Lorentzian (model II) formation probability in eq.(19), ϵ increases initially linearly with proper time until $\tau_0 \sim 1/\langle m_\perp \rangle$ and then eventually decrease as $1/\tau$ due to one dimensional longitudinal expansion.

The inclusive distribution (13) evolves in this case as

$$\begin{aligned} \frac{dN(t)}{dyd^2\mathbf{p}_\perp} &= \mathrm{ch}(y) \int dz \frac{\delta(\eta - y)}{\tau} P(m_\perp \tau) g(\mathbf{p}_\perp) \\ &= g(\mathbf{p}_\perp) P\left(\frac{m_\perp t}{\mathrm{ch}(y)}\right) \end{aligned} \tag{25}$$

showing that partons are formed according to a time dilated formation probability. The transverse energy (14) develops as

$$\frac{dE_\perp(t)}{dy} = \langle m_\perp P(m_\perp t/\mathrm{ch}(y))\rangle \tag{26}$$

On the other hand, along a freeze-out proper time surface $\tau = \tau_f$, the inclusive distribution (15) is given by

$$\frac{dN(\tau_f)}{dyd^2\mathbf{p}_\perp} = g(\mathbf{p}_\perp) P(m_\perp \tau_f) \;\; . \tag{27}$$

Thus g is the asymptotic invariant parton distribution in the free streaming case. The final transverse energy per unit rapidity (16) is

$$\begin{aligned} \mathrm{e}_\perp(\tau_f) &\equiv \frac{dE_\perp(\tau_f)}{dy} = \int \tau_f d\eta d^2\mathbf{x}_\perp \int d^2\mathbf{p}_\perp m_\perp^2 \mathrm{ch}\xi \; f(x,p) \\ &= \langle m_\perp P(m_\perp \tau_f)\rangle = (\tau_f \pi R^2) \; \epsilon_0(\tau_f) \end{aligned} \tag{28}$$

On account of (24), $dE_\perp/dy$ tends toward a constant after the formation era. The last line is just the familiar Bjorken formula relating the observable $dE_\perp/dy$ to the energy density at the freeze-out proper time τ_f.

2.2.1 Free Streaming with Thermal Initial Conditions

In order to study the influence of more realistic finite width of the $\eta - y$ initial state correlations, it is instructive to start with local thermalized source

$$S_{th}(\tau, \xi, p_\perp) = \delta(\tau - \tau_0) F\left(\frac{p_\perp \mathrm{ch}\xi}{T_0}\right) \tag{29}$$

where, eg., $F(x) = ce^{-x}$. For such a source, the solution of the free streaming transport equation is

$$f_1(\tau, \bar{\xi}(\tau; \tau_0, \xi), p_\perp) = \theta(\tau - \tau_0) F\left(\frac{p_\perp \mathrm{ch}\xi}{T_0}\right) \quad , \tag{30}$$

and therefore inverting with (4),

$$f_1(\tau, \xi, p_\perp) = \theta(\tau - \tau_0) F\left(\frac{p_\perp}{T_0} \mathrm{ch}\bar{\xi}(\tau_0; \tau, \xi)\right) \quad , \tag{31}$$

where

$$\mathrm{ch}\bar{\xi}(\tau_0; \tau, \xi) = \left(1 + (\tau/\tau_0)^2 \mathrm{sh}^2\xi\right)^{1/2} \quad . \tag{32}$$

The free streaming energy density in this case is

$$\epsilon_1(\tau) \;=\; \int d\xi d^2\mathbf{p}_\perp \, p_\perp^2 \mathrm{ch}^2\xi f_1(\tau, \xi, p_\perp) = \theta(\tau - \tau_0)\epsilon(\tau_0)\frac{\tau_0}{\tau} h\left(\tau_0/\tau\right) \quad , \tag{33}$$

where the function h modulating the Bjorken τ_0/τ factor is the same as the one defined in [22, 23]:

$$\begin{aligned} xh(x) \;&\equiv\; w(x) = x^4 \int_{-\infty}^{\infty} \frac{d\xi}{2} \frac{\mathrm{ch}^2\xi}{(x^2 + \mathrm{sh}^2\xi)^2} = \frac{x}{2}\left(x + \frac{\sin^{-1}\sqrt{1-x^2}}{\sqrt{1-x^2}}\right) \\ &\approx\; 1 - \frac{4}{3}(1-x) + \frac{2}{5}(1-x)^2 + \cdots \quad . \end{aligned} \tag{34}$$

For large times, $x \to 0$ and

$$xh(x) \to \frac{\pi}{4} x \quad . \tag{35}$$

The factor $\pi/4$ is characteristic of the difference between the isotropic and inside-outside correlated phase space. The energy density at late times follows Bjorken formula reduced by this factor, $\epsilon(\tau) \approx \frac{\pi}{4}\epsilon(\tau_0)(\tau_0/\tau)$. The initial local thermal energy density is given by

$$\epsilon(\tau_0) = \int d\xi d^2\mathbf{p}_\perp \; p_\perp^2 \mathrm{ch}^2\xi F(p_\perp \mathrm{ch}\xi/T_0) = K_{SB}T_0^4 \quad , \tag{36}$$

where the Stefan-Boltzmann constant is

$$K_{SB} = 4\pi \int_0^\infty dx x^3 F(x) \quad . \tag{37}$$

The transverse energy per unit rapidity is closely related to the energy density as seen in eq.(16).

$$\mathrm{e}_\perp^1(\tau) \;\; = \;\; (\tau\pi R^2) \int d\eta d^2\mathbf{p}_\perp p_\perp^2 \mathrm{ch}\xi \; f_1(\tau, \xi, \mathbf{p}_\perp) \quad . \tag{38}$$

This differs from $\epsilon_1(\tau)$ in eq.(33) by only one power less of $\mathrm{ch}\xi$ in the integrand. Noting that

$$\int_{-\infty}^{\infty} \frac{d\xi \mathrm{ch}\xi}{\mathrm{ch}^4\bar{\xi}(t;\tau,\xi)} = \frac{\pi}{4}\frac{t}{\tau} \quad , \tag{39}$$

the transverse energy per unit rapidity remains a constant during free streaming

$$\mathrm{e}_\perp^1(\tau) \;\; = \;\; \frac{\pi}{4}(\tau_0\pi R^2)\epsilon(\tau_0) = \lim_{\tau\to\infty}(\tau\pi R^2)\epsilon_1(\tau) \quad , \tag{40}$$

unlike the energy density. The Bjorken relation between $\mathrm{e}_\perp$ and ϵ is recovered in this case only at large times, after the initial local isotropic conditions evolve toward the ideal $\xi = 0$ case.

2.3 Collisions in the Relaxation Time Approximation

The simplest way to extend the free streaming analysis to include the effects of collisions in eq.(1) is via a relaxation time approximation[21, 22]:

$$C(x,p) = -(pu)(f - f_{eq})/\tau_c(x) \tag{41}$$

where the equilibrium distribution, $f_{eq}(x,p)$ is constrained by energy momentum conservation ($\partial Tu = 0$) to obey

$$\int \frac{d^3\mathbf{p}}{p^0} p^\mu (pu)(f - f_{eq})/\tau_c = 0 \ . \tag{42}$$

While the relaxation time approximation is strictly valid only for small deviations from local equilibrium, it provides one important limit where the general nonlinear transport equations encoded in parton cascade models can be subjected to an analytic test.

With longitudinal boost invariant boundary conditions the equilibrium distribution depends only on (pu) and the local temperature $T(\tau)$,

$$f_{eq}(x,p) = F\left(\frac{pu}{T(\tau)}\right) = f_{eq}\left(\frac{m_\perp \mathrm{ch}\xi}{T(\tau)}\right) \ . \tag{43}$$

Eq. (42) then constrains the temperature to evolve as

$$\epsilon(\tau) = \epsilon_{eq}(\tau) = K_{SB} T^4(\tau) \tag{44}$$

as long as τ_c is assumed to be independent of p.

The transport equation along the characteristic $\bar{\xi}(t;\tau,\xi)$ that passes through ξ at proper time τ is

$$\frac{d}{dt} f(t,\bar{\xi}(t;\tau,\xi),\mathbf{p}_\perp) = -\gamma_c(\tau)(f - f_{eq})(t,\bar{\xi}(t;\tau,\xi),\mathbf{p}_\perp) + S(t,\bar{\xi}(t;\tau,\xi),\mathbf{p}_\perp) \ . \tag{45}$$

This is solved[22] using $e^{-\beta}\partial_\tau(e^\beta f)$ to shift $\gamma_c f$ to the left hand side of the equation taking

$$\beta_c(\tau) = \int_0^\tau dt \gamma_c(t) \ , \tag{46}$$

in terms of the collision rate

$$\gamma_c(\tau) = \tau_c^{-1}(\tau) = \dot{\beta}_c(\tau) \tag{47}$$

The collision rate is assumed to vanishes at $\tau = 0$ for our boundary conditions.

The integral equation for the phase space density is therefore

$$e^{\beta_c(\tau)} f(\tau,\xi,\mathbf{p}_\perp) = \int_0^\tau dt e^{+\beta_c(t)} \left(\dot{\beta}_c(t) f_{eq}(t,\bar{\xi}(t;\tau,\xi),p_\perp) \ + \ S(t,\bar{\xi}(t;\tau,\xi),\mathbf{p}_\perp)\right) \ . \tag{48}$$

Defining the scattering kernel $K(t,\tau)$ via

$$K(t,\tau) = \dot{\beta}_c(t) e^{\beta_c(t)-\beta_c(\tau)} = \gamma_c(t) \exp\left(-\int_t^\tau \frac{dt'}{\tau_c(t')}\right) \quad , \tag{49}$$

the integral equation for f can be written as follows:

$$f(\tau,\xi,\mathbf{p}_\perp) = \int_0^\tau dt K(t,\tau) \left(f_{eq}(t,\bar{\xi}(t;\tau),p_\perp) + \tau_c(t) S(t,\bar{\xi}(t;\tau),p_\perp)\right) \quad . \tag{50}$$

Note that the kernel tends toward $\delta(t-\tau)$ in the rapid thermalization limit, $\tau_c(\tau) \to 0$, and that in that case $f \to f_{eq}$ in the source free region.

For the special case of boost invariant thermal initial conditions, eq.(29), f evolves for $\tau > \tau_0$ according to

$$\begin{aligned} f(\tau,\xi,\mathbf{p}_\perp) &= \theta(\tau-\tau_o) e^{\beta_c(\tau_0)-\beta_c(\tau)} F(p_\perp \mathrm{ch}\bar{\xi}(\tau_0;\tau)/T_0) \\ &\quad + \int_{\tau_0}^\tau dt K(t,\tau) f_{eq}(p_\perp \mathrm{ch}\bar{\xi}(t;\tau)/T(t)) \quad . \end{aligned} \tag{51}$$

This also shows how the system forgets its initial condition as it tries to evolve toward local thermal equilibrium. Whether it get close to f_{eq} or how far it lags behind depends of course on the functional form of the collision rate $\gamma_c(\tau)$.

3 Evolution of the Energy Density

The integral equation for the proper energy density is obtained by integrating eq.(50) using

$$\epsilon(\tau) = \int d\xi d^2\mathbf{p}_\perp p_\perp^2 \mathrm{ch}^2\xi \; f(\tau,\xi,\mathbf{p}_\perp) \quad . \tag{52}$$

This leads to

$$\epsilon(\tau) = \int_0^\tau dt K(t,\tau) \int d\xi d^2\mathbf{p}_\perp p_\perp^2 \mathrm{ch}^2\xi \; \left(f_{eq}(t,\bar{\xi}(t;\tau),p_\perp) + \tau_c(t) S(t,\bar{\xi}(t;\tau),p_\perp)\right) \tag{53}$$

The transverse momentum and ξ integration over f_{eq} can be done as in section2.3 yielding a factor $K_{SB}T^4(t)w(t/\tau)$. The main simplification arises

as a result of the constraint (44) that allows us to replace $K_{SB}T^4(t)$ by $\epsilon(t)$. Therefore,

$$\epsilon(\tau) \;=\; \int_0^\tau dt K(t,\tau)\left(\epsilon(t)w(t/\tau)+\tau_c(t)\bar{\sigma}(t)\right) \quad , \tag{54}$$

where the source term depends on the form of the formation ξ correlations via

$$\bar{\sigma}(t) = \int d\xi d^2\mathbf{p}_\perp p_\perp^2 \mathrm{ch}^2\xi \; S(t,\bar{\xi}(t;\tau,\xi),\mathbf{p}_\perp) \quad . \tag{55}$$

For ideal $\xi = 0$ correlations, $\bar{\sigma}$, reduces to eq.(23). For a thermal correlated source as in, eq.(29), $\bar{\sigma}$ reduces to $\sigma(t)$ modulated by the same $w(t/\tau)$ factor, (34), as the $\epsilon(t)$ term in (54):

$$\begin{aligned}\epsilon(\tau) &= \int_0^\tau dt K(t,\tau)w(t/\tau)\left(\epsilon(t)+\tau_c(t)\sigma(t)\right) \\ &= \theta(\tau-\tau_0)\epsilon(\tau_0)\;\tau_c(\tau_0)K(\tau_0,\tau)\;w(\tau_0/\tau) \\ &\qquad + \int_0^\tau dt K(t,\tau)w(t/\tau)\epsilon(t) \quad .\end{aligned} \tag{56}$$

In the free streaming limit, $\tau_c \to \infty$, $K \to 0$ but $\tau_c K \to 1$. In that limit ϵ reduces to ϵ_1 in eq.(33). In the opposite, rapid thermalization limit (56) reduces to hydrodynamics as we show in the next section.

3.1 Navier-Stokes Limit: Constant τ_c

In the limit of rapid thermalization, $\tau_c \to 0$ we can expand eq.(56) in a power series in τ_c. Consider first the case where τ_c independent of time[21, 22]. In this case

$$K(t,\tau) = e^{(t-\tau)/\tau_c}/\tau_c \quad . \tag{57}$$

The kernel is highly peaked at $t = \tau$. Thus for slowly varying functions, $F(t)$ we can systematically expand

$$\begin{aligned}\int_0^\tau dt\; K(t,\tau)F(t) &= \int_0^{\tau/\tau_c} dx e^{-x}(F(\tau)-\tau_c x\dot{F}(\tau)+\frac{1}{2}\tau_c^2x^2\ddot{F}(\tau)+\cdots \\ &= F(\tau)-\tau_c\dot{F}(\tau)+\tau_c^2\ddot{F}(\tau)+\cdots\end{aligned} \tag{58}$$

The formal expansion of (56) to second order in τ_c then leads to

$$\begin{aligned}\epsilon(\tau) &= \epsilon(\tau) - \tau_c(\dot{\epsilon} + \frac{4}{3}\frac{\epsilon}{\tau} - \sigma(\tau)) \\ &\quad +\tau_c^2(\ddot{\epsilon} + \frac{8}{3}\frac{\dot{\epsilon}}{\tau} + \frac{4}{5}\frac{\epsilon}{\tau^2} - \dot{\sigma} - \frac{4}{3}\frac{\sigma}{\tau}) \ ,\end{aligned} \tag{59}$$

where we $w(1) = 1, \dot{w}(1) = 4/3, \ddot{w}(1) = 4/5$ has been used.

The full integral equation eq.(56) reduces in this case to

$$\left(\dot{\epsilon} + \frac{4}{3}\frac{\epsilon}{\tau} - \sigma\right) = \tau_c\left(\ddot{\epsilon} + \frac{8}{3}\frac{\dot{\epsilon}}{\tau} + \frac{4}{5}\frac{\epsilon}{\tau^2} - \dot{\sigma} - \frac{4}{3}\frac{\sigma}{\tau}\right) + O(\tau_c^2) \tag{60}$$

To lowest order in τ_c, (60) reduces to the Euler hydrodynamic equations for Bjorken boundary conditions

$$\dot{\epsilon} \approx -\frac{4}{3}\frac{\epsilon}{\tau} + \sigma + O(\tau_c) \ . \tag{61}$$

Thus to lowest order

$$\ddot{\epsilon} \approx \frac{4}{3}\left(\frac{4}{3} + 1\right)\frac{\epsilon}{\tau^2} + \dot{\sigma} - \frac{4}{3}\frac{\sigma}{\tau} + O(\tau_c) \ . \tag{62}$$

The first order correction term can therefore be simplified using

$$\ddot{\epsilon} + \frac{8}{3}\frac{\dot{\epsilon}}{\tau} + \frac{4}{5}\frac{\epsilon}{\tau^2} = \frac{4}{3}\frac{4}{15}\frac{\epsilon}{\tau^2} + \dot{\sigma} + \frac{4}{3}\frac{\sigma}{\tau} + O(\tau_c) \ . \tag{63}$$

Note that the $\dot{\sigma}$ terms in (60) cancel, and eq.(60) reduces to the Navier-Stokes, viscous hydrodynamic equation

$$\dot{\epsilon} + \frac{4}{3}\frac{\epsilon}{\tau} = \frac{4}{3}\frac{\eta}{\tau^2} \ + \ \sigma(\tau) \ + \ O(\tau_c^2) \ , \tag{64}$$

with the expected[24, 19] shear viscosity coefficient given by

$$\eta = \frac{4}{15}\tau_c\epsilon \ . \tag{65}$$

For constant τ_c it is clear that viscous corrections can be neglected at large times.

3.2 Navier-Stokes in the Scaling Limit: $\tau_c = \tau/\alpha$

For the Bjorken boundary conditions, however, the proper density $\rho = (uJ)$ decreases as $\rho(\tau) = \tau_0\rho(\tau_0)/\tau$ due to longitudinal expansion. Consequently, the collision rate is expected to scale[23] as

$$\gamma_c = \tau_c^{-1} = \langle \sigma_t \rho(\tau) \rangle \equiv \alpha/\tau \tag{66}$$

The coupling parameter that controls the rate of thermalization is in this case approximately constant

$$\alpha = \langle \sigma_t \rho(\tau_0)\tau_0 \rangle = \tau_0/\tau_c(\tau_0) \tag{67}$$

where σ_t is the transport cross section, and τ_0 is any time after the source is negligible. For a finite formation probability, such as in eq.(19), α must initially grow from zero. In this section we ignore this initial time dependence of α to simplify the analytic treatment. In this scaling regime, the kernel is

$$K(t,\tau) = \frac{\alpha}{t}\left(\frac{t}{\tau}\right)^{\alpha} \tag{68}$$

The integral equation (56) for the energy density reduces to [23]

$$\epsilon(\tau) = \alpha \int_0^\tau \frac{dt}{t}\left(\frac{t}{\tau}\right)^{\alpha+1} h(t/\tau)(\epsilon(t) + t\sigma(t)/\alpha) \tag{69}$$

For $\alpha \gg 1$ the kernel is strongly peaked near $t = \tau$, and we can expand, analogous to eq.(58), in powers of $1/\alpha$

$$\begin{aligned} \int_0^\tau dt\, K(t,\tau)F(t) &= \alpha \int_0^1 dx x^{\alpha-1} F(\tau - \tau(1-x)) \\ &\stackrel{\alpha\to\infty}{\longrightarrow} F(\tau) - \frac{\tau\dot{F}(\tau)}{\alpha+1} + \frac{\tau^2\ddot{F}(\tau)}{(\alpha+1)(\alpha+2)} + \cdots \\ &= F(\tau) - \frac{\tau\dot{F}(\tau)}{\alpha} + \frac{\tau\dot{F}(\tau) + \tau^2\ddot{F}(\tau)}{\alpha^2} + O(\frac{1}{\alpha^3}) \end{aligned} \tag{70}$$

.

The source term expanded to second order in this case is

$$\frac{\tau\sigma}{\alpha} - \frac{\tau^2\dot{\sigma} + \frac{7}{3}\tau\sigma}{\alpha^2} + O(1/\alpha^3) \ , \tag{71}$$

while the energy density term expands to

$$\epsilon - \frac{1}{\alpha}(\tau\dot{\epsilon} + \frac{4}{3}\epsilon) + \frac{1}{\alpha^2}\left(\tau^2\ddot{\epsilon} + \frac{11}{3}\tau\dot{\epsilon} + \frac{32}{15}\epsilon\right) + O(\frac{1}{\alpha^3}) \quad . \tag{72}$$

At $O(1/\alpha)$, we again recover the Euler hydrodynamic equation (61). To next order we recover the Navier-Stokes equation (64) with a time dependent viscosity

$$\eta(\tau) = \frac{4}{15}\frac{\tau\epsilon}{\alpha} = \frac{4}{15}\tau_c(\tau)\epsilon(\tau) \quad . \tag{73}$$

This has the same form as in (65) except that τ_c is here time dependent.

The most interesting point associated with the scaling Navier-Stokes is that unlike in the constant τ_c case (64), the viscosity term does not become negligible compared to the pressure term ($\frac{1}{3}\epsilon/\tau$) at late times. Dissipation in this case decreases the effective speed of sound from $c_s^2 = 1/3$, appropriate for an ideal ultra-relativistic gas, to

$$c_s^2 = \frac{1}{3}\left(1 - \frac{16}{15\alpha}\right) \quad . \tag{74}$$

As discussed in [23], this implies that the energy density in the source free region always decreases more slowly than Euler hydrodynamics predicts:

$$\epsilon(\tau) = \epsilon(\tau_0)\left(\frac{\tau_0}{\tau}\right)^{\frac{4}{3}-\frac{16}{45\alpha}} \quad . \tag{75}$$

It is important to emphasize however, that the Navier-Stokes approximation can only apply if the viscous term is small compared to the pressure term. This requires

$$\alpha \approx \frac{\sigma}{\pi R^2}\frac{dN}{dy} > 1 \quad . \tag{76}$$

This condition is certainly violated at early times when dN/dy is small. In addition, as we will see, this condition is not satisfied in a dense parton gas if the screened cross sections are as small as pQCD estimates would indicate. The detailed study of deviations of kinetic theory and parton cascade solutions from Navier-Stokes solutions is useful as a gauge of whether particular observables such as transverse energy can be correctly interpreted in terms of thermodynamic concepts.

4 Evolution of $\mathrm{e}_\perp(\tau) = dE_\perp/dy$

The transverse energy per unit rapidity is related to the phase space density via eq.(38). For the case of local equilibrium,

$$\mathrm{e}_\perp^{eq}(\tau) = \int \tau d\xi d^2\mathbf{x}_\perp \int d^2\mathbf{p}_\perp p_\perp^2 \mathrm{ch}\xi \; f_{eq}(p_\perp \mathrm{ch}\xi/T(\tau)) = \frac{\pi}{4}(\tau\pi R^2)\epsilon_{eq}(\tau) \quad . \quad (77)$$

The integral equation for $\mathrm{e}_\perp$ is analogous to (53) involving one power less of $\mathrm{ch}\xi$ in the integrand

$$\begin{aligned} \mathrm{e}_\perp(\tau) &= \int_0^\tau dt K(t,\tau) \int d\eta d^2\mathbf{p}_\perp (\tau\pi R^2) p_\perp^2 \mathrm{ch}\xi \\ &\quad \Big(f_{eq}(t, \bar{\xi}(t/\tau,\xi), p_\perp) + \tau_c(t) S(t, \bar{\xi}(t/\tau,\xi), \mathbf{p}_\perp) \Big) \quad . \end{aligned} \quad (78)$$

Because of eq.(39) the integral over f_{eq} gives $\int K(t,\tau) e_\perp^{eq}(t)$ without the weight function w of eq.(34).

For local thermally correlated sources, in particular, the integral equation reduces to

$$\mathrm{e}_\perp(\tau) = \theta(\tau - \tau_0)\mathrm{e}_\perp(\tau_0)\, \tau_c(\tau_0) K(\tau_0,\tau) + \int_{\tau_0}^\tau dt K(t,\tau) \mathrm{e}_\perp^{eq}(t) \quad , \quad (79)$$

Unfortunately, we cannot replace $\mathrm{e}_\perp^{eq}(t)$ by $\mathrm{e}_\perp(t)$, as in the case of the energy density evolution equation, because energy conservation only constrains $\epsilon = \epsilon_{eq}$. Therefore, we must first solve the energy density integral equation (56) to compute the temperature, $T(\tau)$, and then use that solution to compute $\mathrm{e}_\perp^{eq}(\tau)$ via (77). Numerically, it is simplest solve (56,79) together in the same loop iterating time steps and keeping track of prior time steps in an updated array of $\epsilon(\tau_n)$

$$\epsilon(\tau_n) = \tau_c(\tau_0) K(\tau_0,\tau) w(\frac{\tau_0}{\tau_n}) \epsilon(\tau_0) + \sum_{i=0}^{n-1} \Delta\tau K(\tau_i,\tau_n) w(\frac{\tau_i}{\tau_n}) \epsilon(\tau_i) \quad (80)$$

$$\mathrm{e}_\perp(\tau_n) = \frac{\pi}{4}\pi R^2 \left(\tau_c(\tau_0) K(\tau_0,\tau) \tau_0 \epsilon(\tau_0) + \sum_{i=0}^{n-1} \Delta\tau K(\tau_i,\tau_n) \tau_i \epsilon(\tau_i) \right) \quad .(81)$$

This system converges very rapidly even for arbitrary time varying relaxation rates, $\gamma_c(\tau)$, not limited to the scaling form, (66). Because of its numerical simplicity we still refer to the solutions of the above system as analytic for tests of parton cascade codes.

5 Illustrative Numerical Tests

In this section we solve the above integral equations for $e_\perp(\tau)$ and compare them to hydrodynamics and parton cascade results for an initial longitudinally boost invariant but thermally correlated parton gas with $e_\perp(\tau_0 = 0.2 \text{ fm}) = 484$ GeV and very high parton density $\rho(\tau_0 = 0.2 \text{ fm}) = 20/\text{fm}^3$ initial conditions for RHIC energies as estimated from HIJING[3] simulations for central $Au + Au$ collisions at $\sqrt{s} = 200$ AGeV.

First we show in Fig. 1 the expected hydrodynamic evolution in the case of Euler non-dissipative and Navier-Stokes approximations. Note that the Euler solution decreases by over a factor of two as expected from previous studies. The transverse energy loss is however reduced as the transport cross section is reduced. For $\sigma_t < 2mb$ (corresponding to $\alpha < 0.8$) the Navier-Stokes approximation fails badly even for this very high initial parton density. In the figure we have in fact replaced the unphysical negative effective pressure in the Navier-Stokes calculation by zero.

In Fig. 2 we compare the kinetic theory solutions of (81) to Navier-Stokes. For $\sigma = 32$ mb ($\alpha = 12.8$) the transport and Navier Stokes solutions are almost identical. However, by $\sigma = 3$ mb, the Navier-Stokes approximation significantly under-predicts the work done during the expansion relative to the kinetic theory solution. The kinetic theory result of course also differs significantly from the ideal Euler hydrodynamic result.

In Figs. 3 and 4 the kinetic theory solutions are compared to one of the newly developed parton cascade models, ZPC [2]. In that model, only elastic scattering is currently implemented with a differential cross section of the form

$$d\sigma/dt = \frac{9\pi\alpha_s^2}{2}(\frac{\mu^2}{s} + 1)/(t - \mu^2)^2 \tag{82}$$

The total cross section is thus independent of energy, $\sigma = 9\pi\alpha_s^2/2\mu^2$. However, the more relevant transport cross section needed for the input to kinetic theory (81) is

$$\sigma_t = \frac{9}{2}\frac{4\pi\alpha_s^2}{s^2}(1 + \mu^2/s)\int_{\mu^2}^{s+\mu^2}\frac{dy}{y}(y - \mu^2)(s + \mu^2 - y) \tag{83}$$

With this s dependence, the average transport cross section changes with time. Numerical results of ZPC for the time evolution of this quantity can

be parameterized by

$$\sigma_t(\tau) = \begin{cases} 1.74 - 0.205/\sqrt{\tau} \text{ mb} & \text{fig.3} \\ 1.80 - 0.255/\sqrt{\tau} \text{ mb} & \text{fig.4} \end{cases} \tag{84}$$

For the physically reasonable values of $\alpha_s = 0.47$ and $\mu = 3$ fm^{-1}, the transport cross section is so small that even though the parton density is very high, the scaling Navier-Stokes parameter $\alpha = 0.7$ is small and thus neither Euler nor Navier-Stokes approximations apply to this problem. The essential point is, however, that the ZPC code successfully reproduces the analytic results.

We note that in these examples the ZPC code was used in the transverse periodic boundary condition mode to eliminate effects of transverse expansion and therefore be directly comparable to the simple analytic results that were obtained assuming transverse translation invariance. Numerical results with finite transverse radius nuclei, show a reduced transverse energy loss that can also be qualitatively understood as due to a more rapid decoupling or freeze-out that occurs in that case[28]. With periodic boundary conditions the system continues to interact for a longer time. For the conditions shown each event takes about one hour to run on a Sparc 20 from $\tau_0 = 0.2$ to $\tau = 6$ fm. The numerical results (solid dots) correspond to averaging 20 events.

In Fig 4 the results obtained by increasing the initial parton density by two (by decreasing the periodic transverse area a factor of two) are shown. These initial conditions involve one half the transport mean free path relative to fig.3 and correspond to the scaling Navier-Stokes parameter $\alpha \approx 1.4$. For the kinetic theory curves the actual time dependent rates of ZPC using (84) were used as input in solving (81). The accurate reproduction by ZPC of the kinetic theory results in this case confirms again the numerical accuracy of the ZPC model in cases far from both free streaming and hydrodynamic limits.

Finally in Fig. 5, we show results where the initial density was again doubled to consider a case with $\alpha \approx 3$ that should closer to the Navier-Stokes regime. In this case we again find that the ZPC and kinetic solutions again coincide remarkably well, and in this case the viscous hydrodynamic solution approximates much better the kinetic theory evolution. Physically the price paid for this agreement is the necessity to increase $\alpha \propto \sigma_t \rho(\tau_0)$ by a factor of four relative to the HIJING estimates. This can be achieved

physically in many ways. One way is to increase the initial mini-jet density by a factor of two (by decreasing the mini-jet scale p_0 in HIJING from 2 to 1 GeV) and at the same time reduce the screening scale from $\mu \approx 0.6$ GeV to approximately 0.3 GeV. This however is strongly contrary to pQCD expectation where $\mu \approx gT$ should be an increasing function of the density.In addition such a small p_0 is inconsistent with the data on $p\bar{p}$ at FNAL energies[3]. One could expect that inelastic $gg \to ggg...$ processes, not yet included into ZPC could increase gluon density somewhat. However, for our chosen initial conditions, $dE_\perp/dy(\tau_0 \sim 0.2 \text{ fm}) \approx 0.5$ TeV in $Au + Au$ with $\rho(\tau_0) \approx 20/\text{fm}^3$ in Fig. 3, the initial energy density is $\epsilon(\tau_0) \sim 17 \text{ GeV}/\text{fm}^3$, instant chemical and thermal equilibrium would imply that the density would be $\rho_{th}(\tau_0) \approx 2T_0^3 \approx 17/\text{fm}^3$. Thus, the initial conditions are in fact close to chemical equilibrium in this case and further gluon multiplication is not likely. It thus appears difficult to approach the Navier-Stokes regime at RHIC energies. At LHC energies initial densities up to a factor of ten higher parton densities may arise and thus collective hydrodynamic behavior should be more easily be achieved.

Aside from providing physical insight into the possible collective behavior parton evolution in nuclear collisions, the above examples serve well to illustrate how our proposed analytic test can be applied to newly developed cascade models as a check of the numerical implementation of kinetic theory.

6 Summary

The evolution of the transverse energy per unit rapidity was computed in kinetic theory for initial conditions of partons that may arise at RHIC energies. This observable is one of the basic probes for collective phenomena and is particularly interesting because Euler hydrodynamic equations predict a factor of two loss associated with work down as the plasma expands. However, with pQCD estimates of the density of mini-jets and the screened pQCD cross sections it appears that local thermal equilibrium may be hard to maintain even if the initial conditions are assumed to be in boost invariant local thermal equilibrium. Kinetic theory provides a microscopic transport theory to evolution far from local equilibrium. The newly developed parton cascade codes therefore appear to be essential to compute realistic signatures in nuclear collisions.

In this paper we proposed a simple analytic test of parton cascade models for idealized longitudinally boost and transverse translation invariant initial conditions, and showed that this test could be implemented at least in the ZPC[2] code. In the course of applying this test, initial discrepancies between the analytic results based on eqs.(81) and numerical ZPC results were found to be useful in debugging the code. A similar test[29] of the preliminary version of the VNI code[4] uncovered an unphysical scattering prescription that led apparently to anti-work. In the final version of that code that prescription was corrected by modifying the low transverse momenta parts of the scattering subroutines so that similar results to the ZPC test were found. The fact that analytic results far from the Navier-Stokes domain could be reproduced by several parton cascade codes is an important step in demonstrating the soundness of the general parton cascade numerical technology[1] being developed for applications to nuclear collisions at RHIC and LHC energies. Our main proposal is to subject all codes at least in the OSCAR[10] repository to such tests.

Acknowledgments:
We are grateful to W. Haxton for support during the INT96/3 Workshop, where this work was initiated and to J. Randrup for support during during a summer 97 LBL/LDRD program, where this work was completed. Extensive discussions with S. Bass, S. Gavin, K. Geiger, S. Pratt, D. Rischke, X.N. Wang, K. Werner are also gratefully acknowledged.

References

[1] Y. Pang, General Cascade Package (GCP), http://rhic.phys.columbia.edu/rhic/gcp/.

[2] B. Zhang, ZPC Parton Cascade, http://nt1.phys.columbia.edu/people/bzhang/ZPC/zpc.html, CU-TP-853, nucl-th/9709009.

[3] X.-N. Wang and M. Gyulassy, *Phys. Rev. D* **44** (1991) 3501. HIJING: Comp. Phys. Comm. 83 (1994) 307; http://www-nsdth.lbl.gov∼xnwang/hijing/.

[4] K. Geiger, VNI 3.1 Event generator:
http://rhic.phys.columbia.edu/rhic/vni/,
BNL-63762, Jan 1997, hep-ph/9701226.

[5] S. Bass, et al, UQMD1.0β, Nucl. Phys. A610 (1996) 116c;
http://www.th.physik.uni-frankfurt.de$\sim$uqmd/uqmd.html.

[6] K. Werner,Physics Reports 232 (1993) 87;
http://www-subatech.in2p3.fr/Sciences/Theorie/venus/venus.html,

[7] Bao An Li and C.M. Ko, ART, Phys.Rev.C52:2037-2063,1995, e-Print Archive: nucl-th/9505016.

[8] B.H. Sa, A. Tai, LUCIEA 2.0, Comput.Phys.Comm. 90 (1995) 125.

[9] H. Sorge, RQMD, Phys. Rev. C52 (1995) 3291,
ftp://skipper.physics.sunysb.edu/pub/rqmd/v23.dir.

[10] Yang Pang, Riken/BNL Research Center OSCAR Web Page,
http://rhic.phys.columbia.edu/rhic/.

[11] H. Sorge, H. Stocker, W. Greiner, Annals Phys. 192:266-306,1989.

[12] G. Peter, D. Behrens and C. C. Noack, *Phys. Rev. C* **49** (1994) 3253.

[13] T. Kodama, S. B. Duarte, K. C. Chung, R. Donangelo and R. A. M. S. Nazareth, *Phys. Rev. C* **29** (1984) 2146;

[14] G. Kortmeyer, W. Bauer, K. Haglin, J. Murray and S. Pratt, it Phys. Rev. C **52** 2714.

[15] B. Zhang and Y. Pang, DOE/ER/40561-298-INT96-21-003, CU-TP-794, nucl-th/9611012 (1996), PRC in press.

[16] R. V. Ruuskanen, *Phys. Lett.* **147B** (1984) 465.

[17] M. Gyulassy and T. Matsui, Phys. Rev. D29 (1984) 419

[18] M. Gyulassy, D. Rischke and B. Zhang, Nucl.Phys A613 (1997) 397.

[19] P. Danielewics and M. Gyulassy, Phys. Rev. D31, 53 (1985); A. Hosoya, K. Kajantie, Nucl.Phys.B250 (9185) 666.

[20] K. J. Eskola and M. Gyulassy, *Phys. Rev. C* **47** (1993) 2329.

[21] G. Baym, Phys. Lett. B138 (84) 18.

[22] K. Kajantie and T. Matsui, Phys. Lett. B164 (85) 373.

[23] S. Gavin, Nucl. Phys. B351 (91) 561.

[24] S.R. de Groot, W.A. van Leewen, Ch. G. van Weert, Relativistic Kinetic Theory, (North Holland Pub.Co, Amsterdam, 1980).

[25] M. Gyulassy and X.-N. Wang, *Nucl. Phys. B* **420** (1994) 583;
X.-N. Wang, M. Gyulassy and M. Plümer, *Phys. Rev. D* **51** (1995) 3436.

[26] Larry McLerran, Raju Venugopalan, Phys.Rev.D49 (94) 2233 ; 3352 ; Phys.Rev. D50 (1994) 2225; Phys.Rev.D53:458-475,1996.

[27] D. H. Rischke, S. Bernard, J. A. Maruhn, *Nucl. Phys. A* **595** (1995) 346.

[28] B. Zhang, Y. Pang, and M. Gyulassy, Proc. RHIC 97 Summer School, ed. S. Kahana, CU-TP-855, nucl-th/9708055.

[29] K. Geiger, private communication.

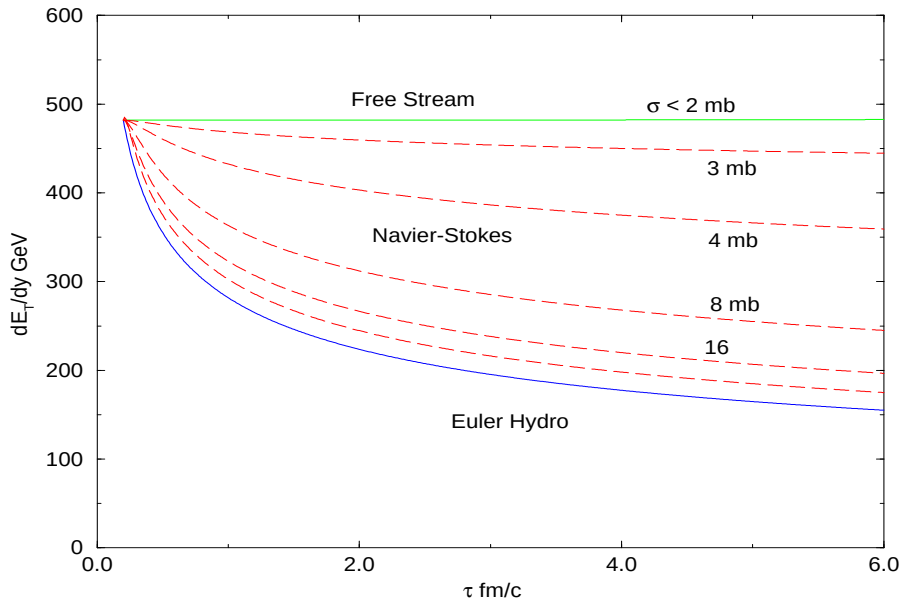

Figure 1: Comparison of the evolution of the transverse energy per unit rapidity in ideal Euler hydrodynamics versus Navier-Stokes dissipative hydrodynamics. The initial conditions were fixed at $\tau = 0.2$ fm to be $dE_\perp/dy = 482$ GeV, $\rho = dN/dy/(\tau A_\perp) = 20/fm^3$. The dependence on the transport cross section via the viscosity coefficient is shown.

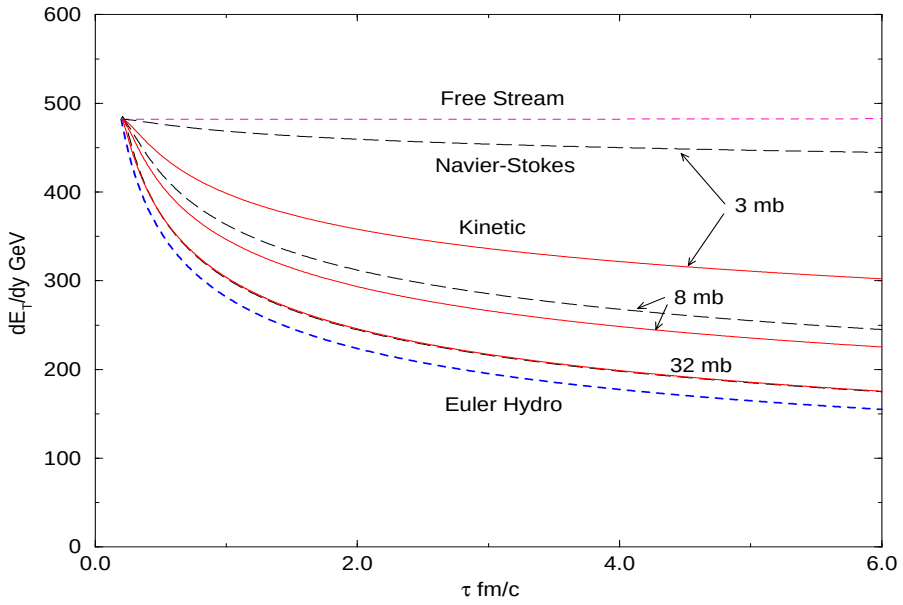

Figure 2: Comparison of kinetic theory evolution to Navier Stokes and Euler hydrodynamics for several cross sections given for the same initial conditions as in fig.1. Note the slow convergence of Navier-Stokes to the kinetic theory result as the transport cross section increases.

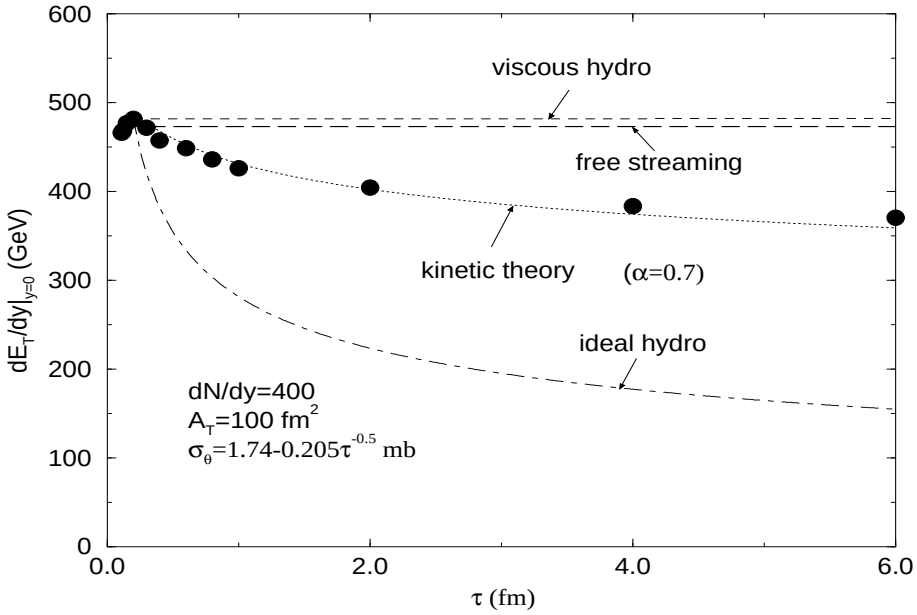

Figure 3: Comparison of analytic kinetic theory results to numerical ZPC code[2] results obtained by averaging 20 events. A periodic transverse grid of dimensions 10 fm was used. Initially (at $\tau = 0.1\ fm$), $T_0 = 500\ MeV$, in an interval $-5 < \eta < 5$, with $\frac{dN}{d\eta} = 400$. The screening mass was assumed to be $\mu = 3\ fm^{-1}$ with a strong interaction coupling constant $\alpha_S = 0.47$. The interaction length for the parton cascade was $0.3\ fm$, and the initial mean free path was $\approx 0.3\ fm$. The comparison starts at $\tau = 0.2\ fm$. The good agreement found with the analytic results confirms the validity of the ZPC algorithm in an interesting case where the exact results deviate strongly from free-streaming and dissipative hydrodynamics.

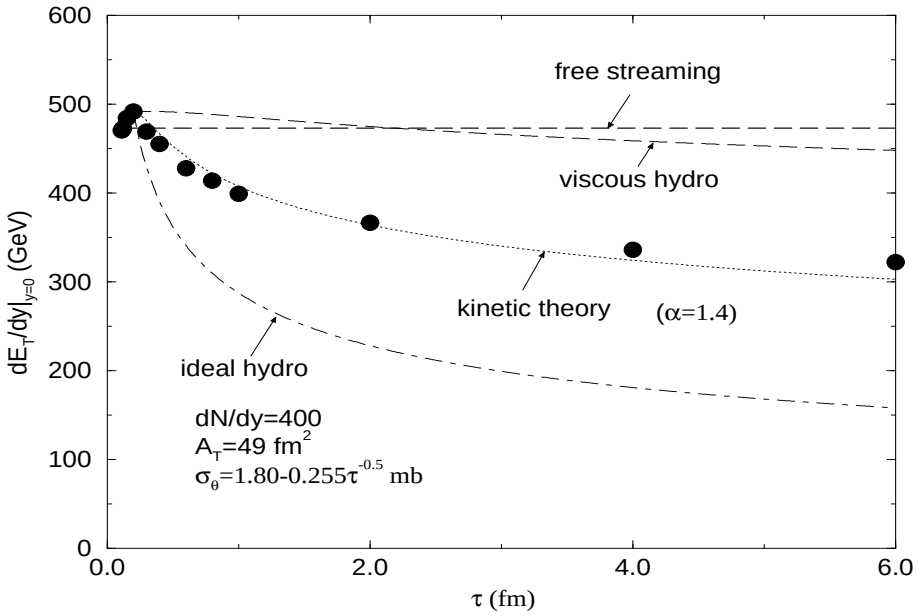

Figure 4: Comparison of ZPC results with analytic kinetic theory for initial conditions with twice as large initial parton density as in Fig. 3. Here the scaling Navier-Stokes with parameter $\alpha = 1.4$, still deviations strongly from the exact kinetic theory results. Nevertheless, good agreement with the numerical ZPC model is again found.

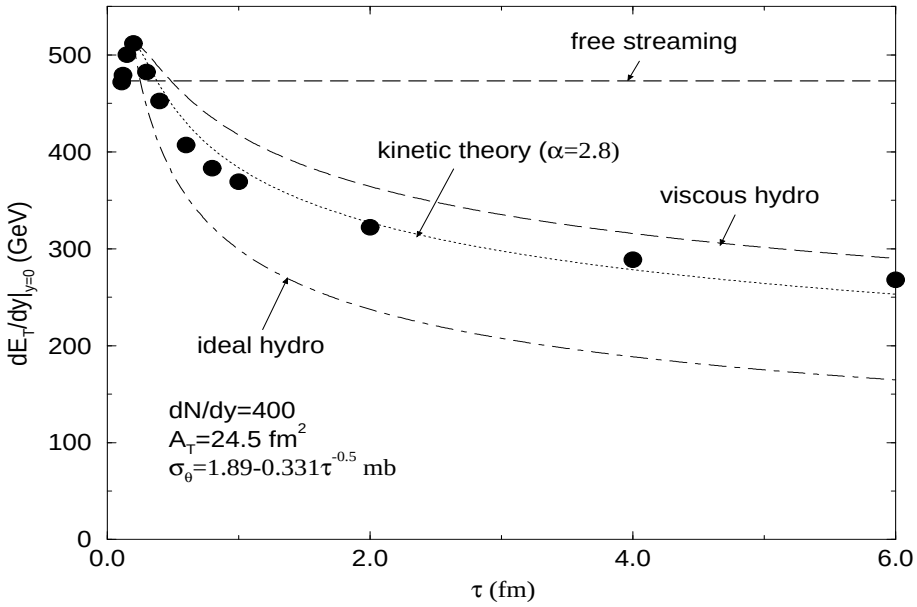

Figure 5: Comparison of ZPC results with analytic kinetic theory and scaling Navier-Stokes for initial conditions with the parameter $\alpha = 2.8$. This demonstrates the ability of the ZPC cascade model to approach the Navier-Stokes dissipative hydrodynamic domain under extreme initial conditions corresponding to four times the default HIJING parton density.